3D Printed Multilayer Microwave Absorber

Wei Zhang, Rui Mi, and Victor Khilkevich*
EMC Laboratory
Missouri University of Science and Technology
Rolla, MO, USA
*khilkevichv@mst.edu

Abstract—**This paper explores the possibility to create 3D printed multilayer electromagnetic absorbers. The proposed design is similar to the thin-film filters used in optics and consists of interleaving high and low permittivity layers. Based on transmission line theory, the multilayer absorber can be designed in a circuit simulator. Analytical equations, circuit simulations, and measurements are used to analyze and validate the designed absorber. Multilayer absorbers based on 3D printed material can be an inexpensive option for engineering usage with great design flexibility and fast fabrication.**

Keywords—Microwave absorber, 3D printed material, multi-layer absorber, transmission line theory

I. Introduction

Microwave absorbers are widely used to shield the high-frequency electromagnetic interference (EMI). In designing microwave absorbers, one needs to consider attenuation, thickness, and bandwidth depending on the application scenario. Commercial absorbers, such as microwave absorbing foam [1], take the advantage of electrically or magnetically lossy materials to make foam structures for broadband absorption. However, to obtain good absorber performance at relatively large effective bandwidths, the thickness of the absorber has to be large enough. For example, for the absorber presented in [2], the thickness of the absorber needs to be greater than 1 cm to achieve reflectivity >17 dB and an effective frequency above 10 GHz.

Frequency selective surfaces (FSS) [3] with resistive surfaces or resistive lumped elements can be designed as microwave absorbers with various bandwidth configurations. In [4], an FSS-based narrow-band absorber with good frequency tolerance and oblique incidence performance was proposed. In addition, an FSS-based multiband absorber was designed in [5]. In [6], broadband FSS absorbers with tunable frequencies are discussed. In addition, ultrathin FSS-based absorbers were designed with wide-band characteristics [7][8].

Moreover, dielectric layered structures were analyzed in the concept of multi-ordered microwave filters [9]. In [10], periodic dielectric structures were discussed in terms of different modeling approaches.

3D printing technology is widely used in many areas due to its flexibility and fast operation. A variety of different 3D printed filaments with different infusion materials are available in the market, so structures with specific electrical properties can be printed for different application scenarios [11-13]. The design of microwave absorbers based on lossy dielectric or FSS structures can take advantage of 3D printing technology, making their fabrication very fast. FSS structures with 3D printed filaments filled with metal particles were proposed by [14]. In [15], the 3D printed FSS absorber was designed based on filaments with lossy carbon materials. Good absorption performance was achieved compared to commercial absorbers.

This paper shows the feasibility of designing multilayer dielectric absorbers above 10 GHz based on the 3D printed material. Using transmission line theory, the reflectivity is calculated numerically or in a circuit simulator. The designed absorber was fabricated, and the synthetic aperture radar (SAR) [15, 16] scan was used to characterize its reflectivity. By using a multilayer structure, an absorber with desired characteristics can be created.

II. Design on Multilayer Absorber

A. Design Methodology

Depending on the structure, narrow-band or broad-band absorbers can be achieved based on 3D printed materials with loss. A basic structure is a single-layer lossy solid sheet with the backside metalized. The reflection coefficient $|S_{11}|$ of the plane wave illuminating the absorber in the normal direction is used to quantify its absorption performance.

A single-layer lossy sheet with a grounded/metalized backside tends to produce relatively narrow periodic absorption bands. Adding extra layers with interleaving high and low permittivity helps to increase the absorption bandwidth by generating more resonances.

The analytical expressions for the reflection coefficient of a multiplayer medium are well known [17, Ch. 4] and can be relatively easily implemented in, for example, Matlab. Alternatively, the same calculation, in a form more convenient for electrical engineers, can be implemented using the transmission line model.

For the multilayer structure shown in Fig. 1, assuming normal incidence of the plane waves to the structure, each layer
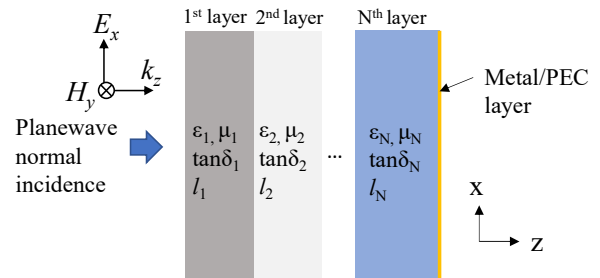

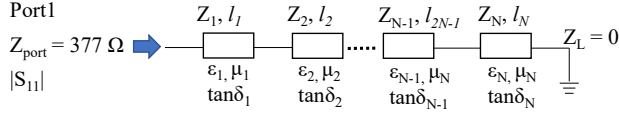Fig. 1. Diagram of the multilayer absorber structure.

Fig. 2. Diagram of the equivalent transmission line model for the multilayer absorber structure.
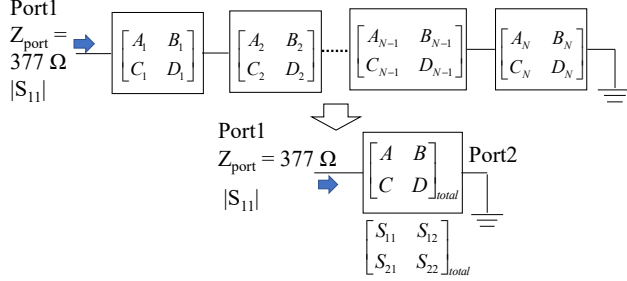

Fig. 3. Diagram of the cascaded ABCD parameter model for the multilayer absorber structure.

of the dielectric can be equated to a transmission line, as shown in Fig. 2. Assuming that the electrical parameters and thicknesses of the material layers are known, the total S-parameters of all layers can be calculated by cascading the ABCD matrices of the layers [18].

For the nth layer, the wave propagation constant γ_n can be expressed as:

$$\gamma_n = j\omega\sqrt{\mu_n\varepsilon_n} \qquad (1)$$

where ω is the frequency of the plane wave; μ_n and ε_n are the permeability and permittivity of the nth layer.

The characteristic impedance of the layer is:

$$Z_n = \sqrt{\frac{\mu_n}{\varepsilon_n}} \qquad (2)$$

For each layer the ABCD matrix can be defined:

$$\mathbf{A}_n = \begin{bmatrix} A & B \\ C & D \end{bmatrix} = \begin{bmatrix} \cosh\gamma_n l_n & Z_n\sinh\gamma_n l_n \\ \frac{1}{Z_n}\sinh\gamma_n l_n & \cosh\gamma_n l_n \end{bmatrix} \qquad (3)$$

where l_n is the thickness of the nth layer. The matrix of the entire structure (Fig. 3) is a product of the layer matrices:

$$\mathbf{A}_{total} = \prod_{n=1}^{N}\mathbf{A}_n \qquad (4)$$

After converting the total ABCD matrix to the total S-parameter matrix, the problem is reduced to the calculation of the reflection coefficient of the two-port network with a short at Port 2. Since the reflection coefficient Γ_L of the short termination at Port 2 is equal to -1, the final expression is the following:

$$S_{11,total} = S_{11} + \frac{S_{21}\Gamma_L S_{21}}{1 - S_{22}\Gamma_L} = S_{11} - \frac{S_{21}^2}{1+S_{22}} \qquad (5)$$

where S_{11}, S_{21}, S_{22} are the elements of the total S-parameter matrix of the layered structure.
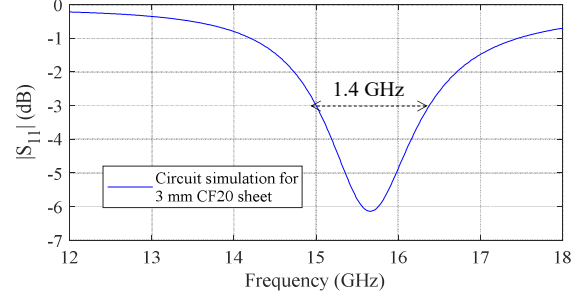

Fig. 4. Reflectivity/Reflection coefficient of the 3 mm CF20 layer with a metal plane at the back side.
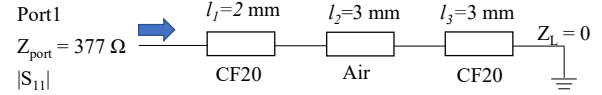

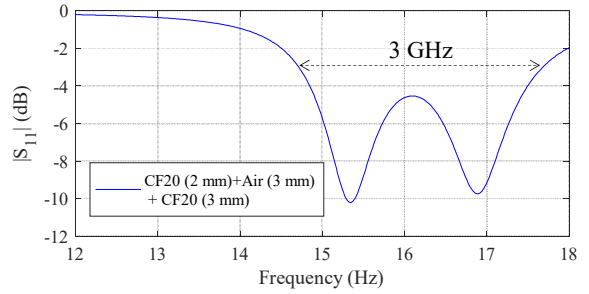Fig. 5. Equivalent transmission line model of the three-layer absorber.

Fig. 6. Reflectivity/Reflection coefficient of the three-layer absorber.

Instead of calculating (5) directly, any circuit simulator allowing to specify arbitrary frequency-dependent values for the impedances and propagation constants of the transmission lines (for example Keysight ADS [19]) can be used to calculate the reflection coefficient of the network in Fig. 2.

B. Multilayer Absorber Design

The 3D printed material used in this paper is a carbon fiber composite material XT-CF20 (CF20) manufactured by ColorFabb [20]. In [21], the electrical parameters of CF20 were measured under different measurement methods including 7 mm coaxial airline [22], capacitance measurement method [23], and open-ended waveguide measurement [22]. In addition, in [21], the measured $|S_{11}|$ of a dielectric resonator is used up to 20 GHz to justify that the permittivity of CF20 is close to constant values of 23 and 6.84 for the tangential and vertical E field relative to the printed layers. In the application scenario studied in this paper, the material CF20 is initially assumed to have the relative permittivity in the x and y direction of about 23 with an electrical loss tangent of about 0.03 in the 10 GHz – 18 GHz frequency range [21]. It has the same magnetic properties as air. For the plane wave normal incidence as shown in Fig. 1, the permittivity in the x direction is considered because the E field is oriented in the x direction.

The reflection coefficient of the single 3 mm layer of the CF20 material calculated using the transmission line model is

Layer 1: 100% CF20   Layer 2: 15% PLA   Layer 3: 100% CF20
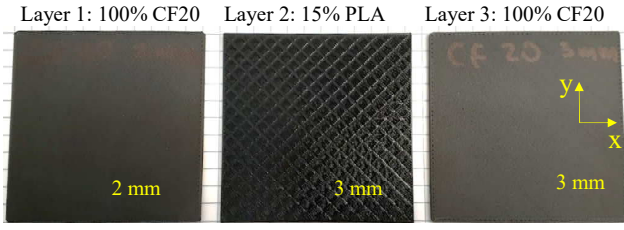
2 mm   3 mm   3 mm

Fig. 7. The 3D printed layers of the designed absorber.

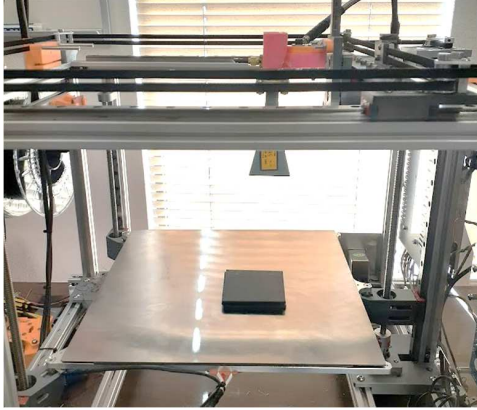

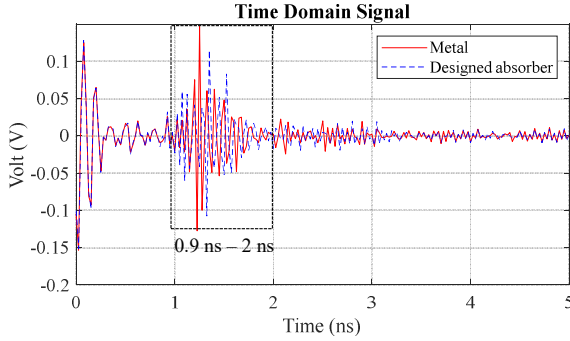Fig. 8. Setup of the SAR reflectivity scan of the designed absorber.

Fig. 9. Time-domain reflected signal at the metal (x = 51 mm, y = 205 mm) and absorber locations (x = 109 mm, y = 103 mm).

shown in Fig. 4. As can be seen, the reflection coefficient has a null at 15.7 GHz with the maximum absorption of 6 dB, but the bandwidth is relatively narrow (1.4 GHz at -3 dB).

Increasing the order of the filter by adding a 3 mm air layer and a 2 mm CF20 layer, as show in Fig. 5, allows to increase the 3 dB bandwidth to 3 GHz (Fig. 6).

By adding more layers, the order of the filter can be further increased leading to increased bandwidth and, potentially, the stop band absorption. However, this is achieved at the expense of increasing the overall thickness of the filter.

III. VALIDATION ON THE DESIGNED 3-LAYER ABSORBER

For the experimental validation, the absorber was fabricated by printing the layers separately using the Jubilee 3D printer [24]. The size of the absorber layers was 7x7 cm. The CF20 layers were printed with 100% rectilinear infill, and the "air"
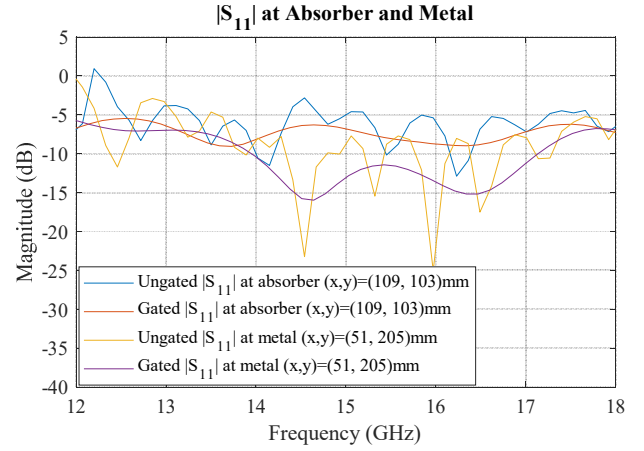

Fig. 10. Ungated and gated $|S_{11}|$ at the metal (x = 51 mm, y = 205 mm) and absorber (x = 109 mm, y = 103 mm) locations.

layer was printed using the PLA material with a low infill ratio (15%). The thickness of top and bottom walls was 1 layer. As the infill ratio of the PLA (dielectric constant: 2.2-2.4 [25]) is 15%, it is assumed the 15% PLA layer shows the effective permittivity close to air. The layers are shown in Fig. 7.

Transmission coefficient (S_{21}) measurement can be used to characterize the microwave absorber material without a metalized backside, such as shielding effectiveness measurement [26]. As the multilayer microwave absorber in this paper was designed with a metalized backside, the SAR reflectivity (reflection coefficient, S_{11}) scan was performed as described in [15]. The 3D printer used to create the absorber was employed to perform the scan as well. To achieve that, a Ku band standard gain horn was attached instead of the printing head and the absorber was placed on the printing bed underneath (Fig. 8).

The antenna was moved within the 250x250 mm area with 40 samples in the X and Y directions (6.4 mm sampling step, 1600 samples in total).

The reflection coefficient or reflectivity as a function of coordinates $S_{11}(x, y)$ is measured by a vector network analyzer (VNA) in the frequency range 12.4 GHz – 18 GHz). It is defined as the ratio of the reflected wave and the incident wave in terms of voltage at the port of the horn antenna when the VNA is calibrated. Since the antenna is not perfectly matched and its reflection is comparable to the reflection from the metal plate placed several centimeters from the antenna aperture, the time-domain gating method [27] was used to remove the unwanted antenna reflections. An example of the measured reflected coefficient in the time domain is given in Fig. 9 with the gating window corresponding to the reflections of the metal plate and the absorber. After removing the antenna reflections in the time domain, an inverse fast Fourier transform (FFT) is performed to convert the reflected signal back to the frequency domain and apply the SAR algorithm. The frequency-domain reflection coefficients at certain sampling locations before and after gating are shown in Fig. 10.

61

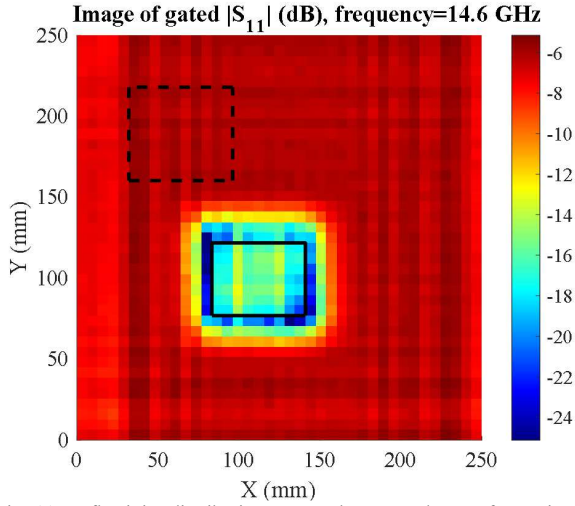**Image of gated |S$_{11}$| (dB), frequency=14.6 GHz**

Fig. 11. Reflectivity distribution among the scanned area after gating at 14.6 GHz and applying the SAR algorithm. Black boxes indicate the averaging regions for the absorber and the plate.
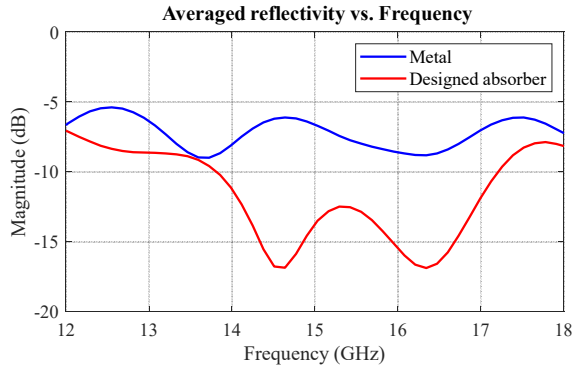

Fig. 12. Gated reflectivity (|S$_{11}$|) after averaging at the metal and absorber areas.

Fig. 13. Comparison of measured and simulated reflectivity (|S$_{11}$|) of the designed absorber (with CF20 relative permittivity of 23 in the simulation).

Fig. 14. Comparison of measured and simulated reflectivity (|S$_{11}$|) of the designed absorber (with CF20 relative permittivity of 25 in the simulation).

Fig. 11 shows a gated reflection coefficient (|S$_{11}$|) image obtained by the SAR algorithm at 14.6 GHz (one of the reflectivity nulls). The location of the absorber on the metal plate can be easily identified, the reflectivity within the absorber region is visually lower than the reflectivity of the metal plate. However, the variations in the reflectivity exist both within the absorber region and on the metal plate. To quantify the overall absorber reflectivity, the absolute values of the reflection coefficient (|S$_{11}$|) image were averaged over the two regions corresponding to the absorber and the metal plate as indicated in Fig. 11 (dashed rectangle for the metal plate and solid rectangle for the absorber).

The average reflection coefficient (|S$_{11}$|) of metal and absorber are compared at different frequencies in Fig. 12. Compared with the metal sheet, the reflectivity of the designed absorber is measured to have a significant absorption capability of up to 10 dB at around 14.6 GHz. It is noted that the absolute value of the average gated reflectivity |S$_{11}$| of metal is not 0 dB (as could be expected). This happens because the S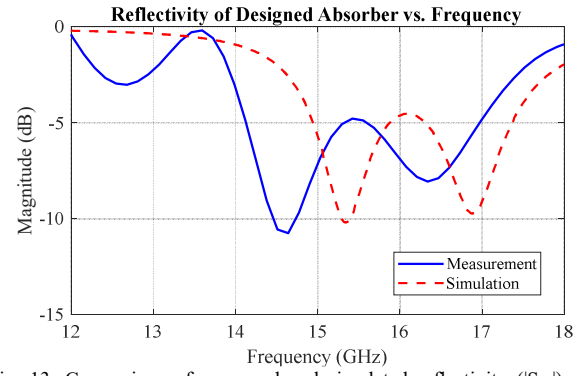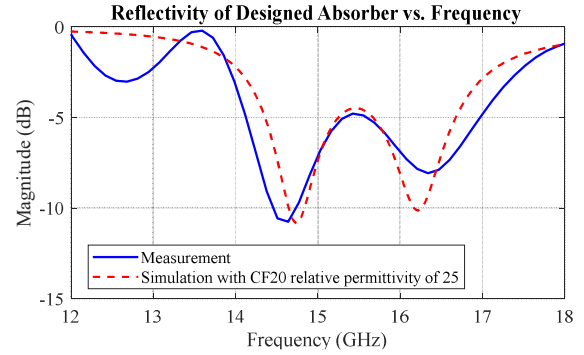AR measurement was not calibrated, for example there was no correction for the reflections from the antenna aperture and non-isotropic antenna radiation pattern.

By normalizing the average reflectivity of the designed absorber to the average reflectivity of metal (i.e., assuming that the absolute value of the reflection coefficient of the metal plate is equal to 1), the relative reflectivity of the designed absorber can be obtained and compared directly to the theoretical values from the previous section. The comparison is shown in Fig. 13. As can be seen, the measured absorption curve agrees well with the curve predicted theoretically. However, a shift in the absorption band is observed. This is because the material parameters of the dielectrics are not known exactly. By changing the value of the CF20 relative permittivity from 23 to 25, it is possible to achieve a better match between the measured and calculated absorber responses. As shown in Fig. 14, the difference in the resonant frequencies between measurement and simulation is within 200 MHz.

IV. CONCLUSION

In this paper, the proof of concept of designing multilayer absorbers based on 3D printed materials is shown. The absorber can be designed based on transmission line models in the circuit simulation. For a 3 mm lossy 3D printed material CF20, better impedance matching, and multiple resonances with expanded absorption bandwidth can be intentionally achieved by adding two additional layers (2 mm CF20 layer and 3 mm air layer).

62

The absorption performance of the fabricated absorber shows a good correlation with the simulated results. The discrepancy of the resonant frequencies between measurement and simulation is within 200 MHz with the relative permittivity of CF20 assumed as 25 up to 18 GHz.

REFERENCES

[1] Laird, Microwave Absorbers, [Online]. Available: https://www.laird.com/products/microwave-absorbers

[2] Laird, RPF-DS-Eccosorb AN 180620, [Online]. Available: https://www.laird.com/sites/default/files/2021-01/RFP-DS-AN%2006242020.pdf

[3] B. A. Munk, Frequency Selective Surfaces: Theory and Design. Hoboken, NJ, USA: Wiley, 2000.

[4] G. I. Kiani, K. L. Ford, K. P. Esselle, A. R. Weily and C. J. Panagamuwa, "Oblique Incidence Performance of a Novel Frequency Selective Surface Absorber," in *IEEE Transactions on Antennas and Propagation*, vol. 55, no. 10, pp. 2931-2934, Oct. 2007, doi: 10.1109/TAP.2007.905980.

[5] A. Omar, H. Huang and Z. Shen, "Multi-Band Absorptive Frequency-Selective Reflection Structures," *2019 Joint International Symposium on Electromagnetic Compatibility, Sapporo and Asia-Pacific International Symposium on Electromagnetic Compatibility (EMC Sapporo/APEMC)*, 2019, pp. 52-54, doi: 10.23919/EMCTokyo.2019.8893882.

[6] Y. Zhang, L. Miao, S. Guo, Z. Huang, Z. Cao, Y. He, J. Wei, C. Li and J. Jiang, "A broadband tunable frequency selective surface absorber for oblique incidence applications," in *Journal of Physics D, Applied Physics*, vol. 53, no. 5, Oct. 2019, Art. no. 055105, doi: 10.1088/1361-6463/ab50f5.

[7] F. Costa, A. Monorchio and G. Manara, "Analysis and Design of Ultra Thin Electromagnetic Absorbers Comprising Resistively Loaded High Impedance Surfaces," in *IEEE Transactions on Antennas and Propagation*, vol. 58, no. 5, pp. 1551-1558, May 2010, doi: 10.1109/TAP.2010.2044329.

[8] J. Zhou, S. Bie, D. Wan, H. Xu, Y. Xu and J. Jiang, "Realization of Thin and Broadband Magnetic Radar Absorption Materials With the Help of Resistor FSS," in *IEEE Antennas and Wireless Propagation Letters*, vol. 14, pp. 24-27, 2015, doi: 10.1109/LAWP.2014.2349533.

[9] Y. Li, I. Liberal and N. Engheta, "Dispersion synthesis with multi-ordered metatronic filters," in *Optics express*, vol. 25, no. 3, pp.1937-1948, Feb. 2017.

[10] J.D. Shumpert, "Modeling of periodic dielectric structures (electromagnetic crystals)," University of Michigan, 2001.

[11] Proto-pasta, Electrically Conductive Composite PLA. [Online]. Available: https://www.proto-pasta.com/products/conductive-pla?variant=1265211476.

[12] Proto-pasta, Iron-filled Metal Composite PLA. [Online]. Available: https://www.proto-pasta.com/products/magnetic-iron-pla?variant=1204196648

[13] AFINIA 3D, Specialty PLA Filament - Aluminum-infused. [Online]. Available: https://store.afinia.com/Specialty-PLA-Filament--Aluminum-infused_p_114.html

[14] R. Kronberger and V. Wienstroer, "3D-printed FSS using printing filaments with enclosed metal particles," in *2017 Progress in Electromagnetics Research Symposium - Fall (PIERS - FALL)*, 2017, pp. 808-811, doi: 10.1109/PIERS-FALL.2017.8293245.

[15] R. Mi, W. Zhang, K. Ghosh, S. Walunj, Q. Liu, J. Rollin, P. Sochoux, D. Pommerenke and V. Khilkevich, "3D Printed Electromagnetic Absorber Built with Conductive Carbon-filled Filament," *2021 IEEE International Joint EMC/SI/PI and EMC Europe Symposium*, 2021, pp. 266-271, doi: 10.1109/EMC/SI/PI/EMCEurope52599.2021.9559309.

[16] C. J. Oliver, "Synthetic-aperture radar imaging," in *J. Phys. D: Appl. Phys.*, vol. 22, no. 7, pp. 871-890, 1989.

[17] E. J. Rothwell and M. J. Cloud, Electromagnetics. Boca Raton, FL, USA: CRC Press, 2001.

[18] D.M. Pozar, Microwave Engineering, John wiley & sons, 2011.

[19] Keysight Technologies, 2020, PathWave Advanced Design System (ADS) 2020. [Online]. Available: https://www.keysight.com/us/en/products/software/pathwave-design-software/pathwave-advanced-design-system.html

[20] ColorFabb, XT-CF20. [Online]. Available: https://colorfabb.com/xt-cf20?gclid=Cj0KCQiAieWOBhCYARIsANcOw0xAhPortfcpzD95WIPmA_NWBvxWT2q9xvevV7LiSr3N8l6e2FcmJ9saAnD2EALw_wcB

[21] A. Harmon, V. Khilkevich, K. M. Donnell, "High Permittivity Anisotropic 3D Printed Material," accepted in *2022 IEEE International EMC+SIPI Symposium*.

[22] Keysight, 85071B Materials Measurement Software User's Manual (Apr93), 1993.

[23] Standard test methods for AC loss characteristics and permittivity (dielectric constant) of solid electrical insulation. ASTM D150-98, 2018.

[24] J. Vasquez, *Jubilee Project wiki*. [Online]. Available: https://jubilee3d.com/index.php?title=Main_Page. [Accessed: 07-Jan-2022].

[25] J. Zechmeister and J. Lacik, "Complex Relative Permittivity Measurement of Selected 3D-Printed Materials up to 10 GHz," 2019 Conference on Microwave Techniques (COMITE), 2019, pp. 1-4,

[26] Y. Liu, R. He, V. Khilkevich and P. Dixon, "Shielding Effectiveness of Board Level Shields with Absorbing Materials," *2019 IEEE International Symposium on Electromagnetic Compatibility, Signal & Power Integrity (EMC+SIPI)*, New Orleans, LA, USA, 2019, pp. 84-89.

[27] B. Archambeault, S. Connor, and J. Diepenbrock, "Time domain gating of frequency domain s-parameter data to remove connector end effects for pcb and cable applications," in *2006 IEEE International Symposium on Electromagnetic Compatibility*, 2006. EMC 2006., vol. 1, pp. 199– 202, IEEE, 2006.

63